International Journal of Mechanical Sciences 115-116 (2016) 190–201

Contents lists available at ScienceDirect

International Journal of Mechanical Sciences

journal homepage: www.elsevier.com/locate/ijmecsci

Analytical model of milling forces based on time-variant sculptured shear surface

Feng Jiang [a,*], Tao Zhang [a], Lan Yan [b]

[a] Institute of Manufacturing Engineering, Huaqiao University, 361021 Xiamen, PR China
[b] College of Mechanical Engineering and Automation, Huaqiao University, 361021 Xiamen, PR China

ARTICLE INFO

Article history:
Received 5 April 2016
Received in revised form
8 June 2016
Accepted 23 June 2016
Available online 24 June 2016

Keywords:
Analytical model
Milling forces
Sculptured shear surface
Geometry of cutting tool
Milling parameters

ABSTRACT

A concept of sculptured shear surface was proposed in this study. The sculptured shear surface is determined by helix structure and movement of milling tool. The area of sculptured shear surface is time variant during milling processes. The projected area of sculptured shear surface in three directions determines the milling forces in three directions respectively. The analytical model of milling forces based on sculptured shear surface is build and this analytical model is verified by the milling experiments. Finally the effect of cutting tool geometrical parameters (helix angle and rake angle) and milling parameters (axial depth of cut, radial depth of cut, feed rate per tooth) on milling forces is analyzed by proposed milling force model.

© 2016 Elsevier Ltd. All rights reserved.

1. Introduction

The research on cutting forces of machining process is necessary and can generate further insight into cutting temperature, tool life, surface finish, and other machinability properties. There are mainly three methods to predict the cutting forces: empirical/semi-empirical methods, finite element methods and analytical methods.

Empirical methods include some statistical relationship models between the cutting forces and cutting parameters, such as exponential model, second order model and so on [1]. The contribution of every item to the cutting forces is different, which results in the coefficient of every item is different. A large amount of experiments are performed to get the cutting forces and then the data is used to fit the coefficient of every considered item [2]. In semi-empirical methods, the analytical models of uncut chip thickness are built, and then the relationship between uncut chip thickness and cutting forces are built [3]. The cutting forces are considered to be proportional to the uncut chip thickness under certain cutting conditions and the ratios were called force component coefficients [4]. These coefficients can be gained from a lot of experiments and the cutting force components are approximated. Further researches showed the relationship between cutting force and chip thickness to be an exponential function. The force coefficients agree with the polynomial model including the cutting process parameters [5]. Beside the force component coefficients, some other coefficients called edge coefficients were proposed in the cutting force model, which make cutting forces model better agreed with the experimental results [6]. The empirical or semi-empirical methods, however sophisticated, are useful in practice process but they are limited to the fixed machine tool, cutting tool and cutting conditions. The predictions of force largely depend on the reliability of the empirical cutting force coefficients, which are gained from a large number of experiments in different cutting conditions. Because the physical meanings of force coefficients are undefined, this kind of model is difficult to reflect the physical process truly and it is difficult to be used widely.

Finite element method (FEM) was more and more popular in the processes simulation from the 1980s onward. FEM is an important tool to study the complex thermo-mechanical phenomenon of cutting process, which is difficult to investigate by experimental measurement. It is used to calculate cutting forces [7], cutting temperature [8] and stress distribution [9], or research the tool design methods and select the optimum cutting conditions [10]; even predict the tool wear process [11] and the residual stresses in the machined layer [12]. Some commercial FEM codes, like ABAQUS [13], DEFORM [14], AdvantEdge [15] are available to use to simulate the cutting processes. The simulated results by finite element methods could be accurate in the predicting of cutting forces as soon as the material model [16], friction model

* Corresponding author.
E-mail address: jiangfeng@hqu.edu.cn (F. Jiang).

http://dx.doi.org/10.1016/j.ijmecsci.2016.06.018
0020-7403/© 2016 Elsevier Ltd. All rights reserved.

[17], heat transfer model [18]and numerical approach [19] is reasonable. However, the prediction of cutting forces is time consuming and the commercial FEM software is too expensive to use widely in the industry.

The above two methods for the prediction of cutting forces are difficult to build the nature and direct relationship between cutting forces and cutting process parameters, including machining parameters, geometrical parameters of cutting tool and so on. Analytical models of cutting forces considers the analysis in the cutting processes, including the materials deformation, flow, contact action and so on. It is generally considered that the source of resultant cutting forces are shearing and friction in the cutting processes [20]. The components of cutting force are derived as projection of the resultant cutting force. The friction forces can be considered as the function of shear forces and friction angle. The shear force is approximately expressed as the product of shear area and shear stress. The friction, shear area and shear stress models are required to solve the cutting forces. Many analytical models of orthogonal cutting were developed, like "card model", "shear angle model" [21], "slip line model" [22], "thermo-stress coupled model" [23] and so on. But in some complex cutting processes, like milling, the shear plane or zone is not a plane, but a curved surface due to complex tool structure and tool movement. Generally the differential elements are obtained by slicing the milling tool along helical cutting edge. It could be considered as orthogonal cutting condition for every discrete element. The milling forces are integrated axially along the sliced differential elements from the bottom of the flute towards the final axial depth of cut. More prediction of cutting forces of complex operations and tool cutting could be performed by the above analytical method [24]. However, the accuracy of the milling force prediction strongly depends on the size of differential elements. The height of differential elements in the axial direction should be small enough to avoid the prediction error of cutting forces. Moreover, it is difficult to analyze the continual and dynamic change of cutting forces due to removal of workpiece materials.

In this study, a concept of sculptured shear surface was proposed. The sculptured shear surface is determined by helix structure and movement of milling tool. The area of sculptured shear surface is time variant during milling processes. The projected area of sculptured shear surface in three directions determines the milling forces in three directions respectively. The analytical model of milling forces based on sculptured shear surface is build and this analytical model is verified by the milling experiments. Finally the effect of cutting tool geometrical parameters (helix angle and rake angle) and milling parameters (axial depth of cut, radial depth of cut, feed rate per tooth) on milling forces is analyzed by proposed milling force model.

2. Milling force model based on sculptured shear surface

2.1. Orthogonal cutting forces system

The cutting forces [25] and velocity system [26] acting in the orthogonal cutting are discussed in many researches, as Fig. 1 shown. The equation of shear force F_s, resultant force R, friction force f and normal pressure N are respectively:

$$F_s = \tau_s \cdot h \cdot a_w / \sin\varphi \tag{1}$$

$$R = F_s / \cos(\varphi + \beta_\alpha - \alpha) \tag{2}$$

$$F_c = \tau_s \cdot h \cdot a_w \cdot \cos(\beta_\alpha - \alpha) / \sin\varphi / \cos(\varphi + \beta_\alpha - \alpha) \tag{3}$$

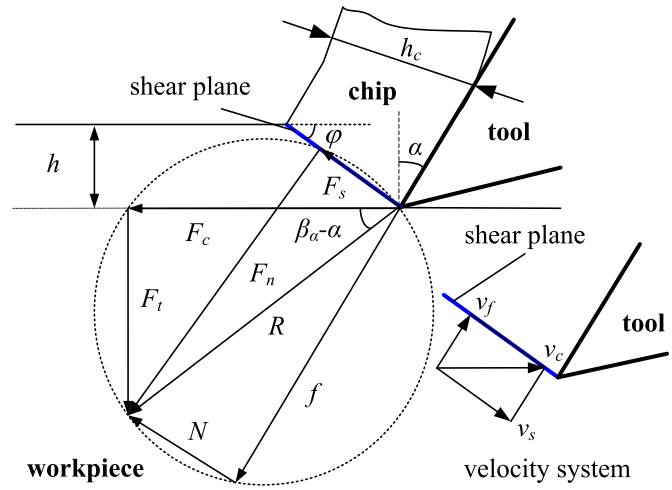

Fig. 1. Orthogonal cutting forces and velocity system.

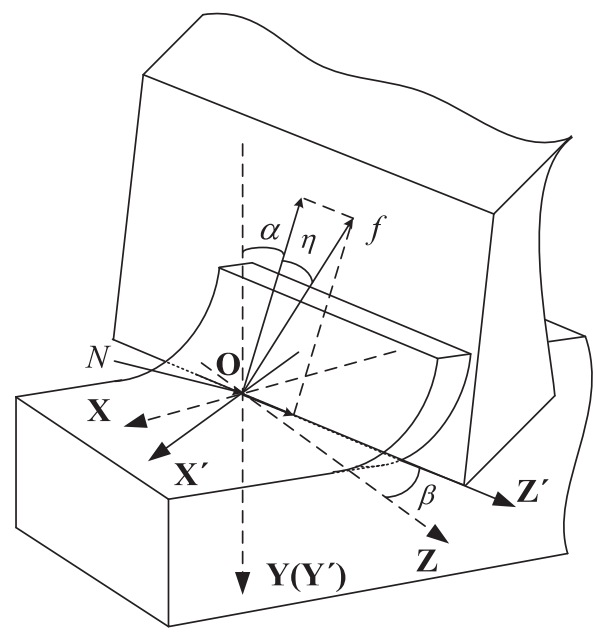

Fig. 2. Oblique cutting model.

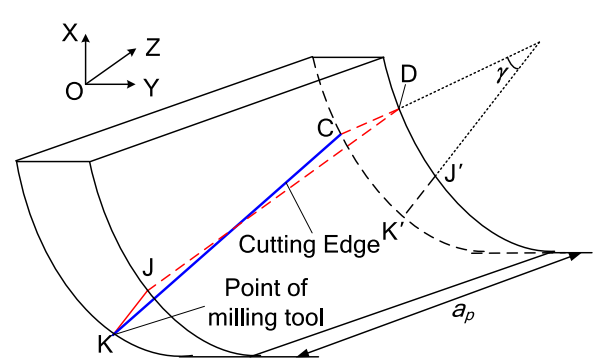

Fig. 3. Physical model of cutting edge and shear curved plane.

$$f = R \cdot \sin\beta_\alpha \tag{4}$$

$$N = R \cdot \cos\beta_\alpha \tag{5}$$

Where a_w is the width of cut; h is the uncut chip thickness; τ_s is the shear stress; ϕ is the shear angle; β_α is the friction angle; α is the rake angle.

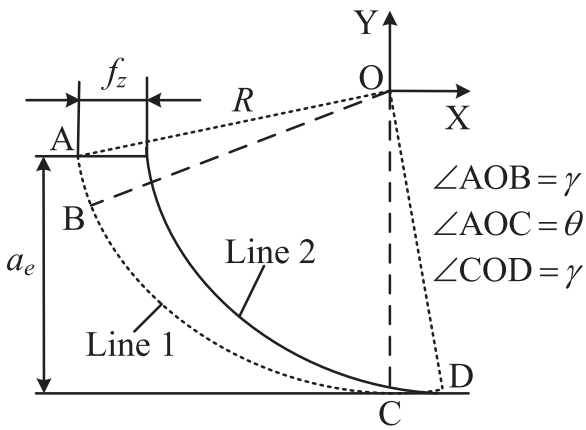

Fig. 4. Cutting stage.

The equation of shear velocity v_s and sliding velocity v_f are expressed as:

$$v_s = v_c \cdot cos\alpha / sin(\pi/2 + \alpha - \varphi) \tag{6}$$

$$v_f = v_c \cdot sin\varphi / sin(\pi/2 + \alpha - \varphi) \tag{7}$$

Where v_c is the cutting speed.

The shear angle is expressed as:

$$\varphi = arctan\left(h \cdot cos\alpha / (h_c - h \cdot sin\alpha)\right) \tag{8}$$

Where h_c is the chip thickness.

2.2. Oblique cutting forces model

The measured cutting forces are generally in the coordinate *XYZ*, as Fig. 2 shown. An auxiliary coordinate *X′Y′Z′* is built to aid the calculation of analytical cutting forces.

In the auxiliary coordinate *X′Y′Z′*, the forces components $F_{X'}$, $F_{Y'}$ and $F_{Z'}$ in the three axes are respectively expressed as [27]:

$$F_{X'} = f \cdot cos\eta \cdot sin(\alpha - \theta + wt) + N \cdot (\alpha - \theta + wt) \tag{9}$$

$$F_{Y'} = f \cdot cos\eta \cdot cos(\alpha - \theta + wt) - N \cdot sin(\alpha - \theta + wt) \tag{10}$$

$$F_{Z'} = f \cdot sin\eta \tag{11}$$

The auxiliary coordinate *X′Y′Z′* is revolved β about *Y′* axis to transform to the coordinate *XYZ*, the forces components $F_{X'}$, $F_{Y'}$ and $F_{Z'}$ in the three axes are respectively expressed as:

$$F_X = F_{Z'} \cdot sin\beta + F_{Z'} \cdot cos\beta \tag{12}$$

$$F_Y = F_{Y'} \tag{13}$$

$$F_Z = F_{Z'} \cdot cos\beta - F_{X'} \cdot sin\beta \tag{14}$$

2.3. Sculptured shear surface

The analytical model of major cutting edge and shear plane is shown in Fig. 3. K is the cutting point of tool and CK is the major cutting edge. The uncut chip thickness which changes from the length of KJ to CD is varied during milling process. CDJK is a spatial curved face which consists of the uncut thickness in every position of the cutting edge. In the milling process, if the cutting tool is sliced to many thin layers along the direction of cutting edge, every layer can be considered to act as oblique cutting. But the depth of cut *h* is varied, equal to the uncut chip thickness *f*(*z*,*t*), which is the function of cutting time *t* and Z direction position *z*.

K′J′ is the projection of KJ to plane *XY*. The line CD and K′J′ meet at the origin O, which is in the axis of cutting tool. Their included angle γ is defined as the phase angle and the expression of γ is:

$$\gamma = a_p \cdot tan\beta / R \tag{15}$$

2.4. Time variant milling force model

2.4.1. Definition of cutting stage

Milling forces are the function of cutting time *t*. As the Fig. 4 shows, cutting tool point K cuts into workpiece at point A and cuts out at point D. The total cutting time is defined as t^*, which is expressed as:

$$t^* = (\theta + \gamma)/\omega \tag{16}$$

$$\gamma = a_p \cdot tan\beta / R \tag{17}$$

The total time t^* is divided into three stages:

1st stage: cutting in stage, part of cutting edge contacts with workpiece materials. Cutting tool point moves from A to B, point B is the critical point between cutting in stage and steady cutting stage. Cutting time $t_1 = \gamma/\omega$;.

2nd stage: steady cutting stage, all the cutting edge contacts with workpiece materials. Cutting tool point moves from B to C. Cutting time $t_2 = (\theta\text{-}\gamma)/\omega$;.

3rd stage: cutting out stage, part of cutting edge contacts with workpiece materials. Cutting tool point moves from C to D, point C is the critical point between steady cutting stage and cutting out stage. Cutting time $t_3 = \gamma/\omega$.

2.4.2. Cutting forces model in 1st stage

As shown in Fig. 5, the uncut chip thickness is expressed as:

$$f(z,t) = f_z \cdot sin(\theta - \omega \cdot t + z \cdot tan\beta / R),\ 0 \le z \le a_p' = R \cdot \omega \cdot t \cdot ctan\beta \tag{18}$$

The differential sliced layers are integral along the direction of cutting edge (*Z* direction) and the total shear force is expressed as:

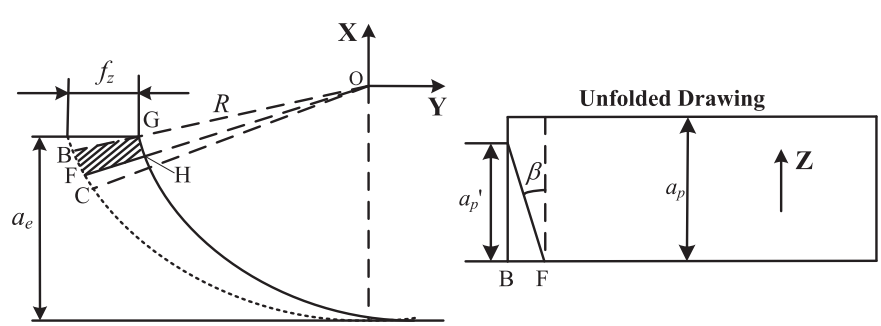

Fig. 5. 1st cutting edge.

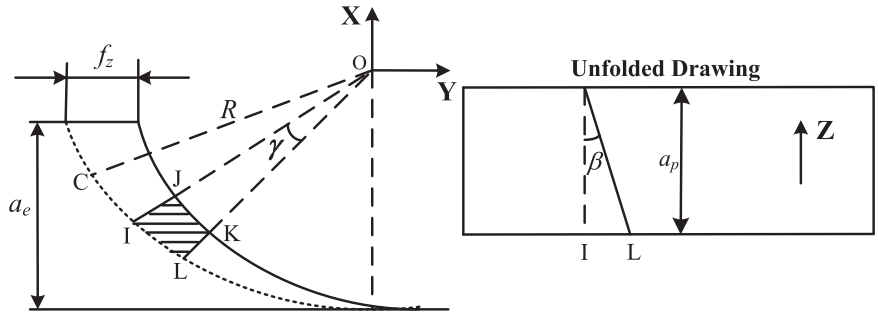

Fig. 6. 2nd cutting edge.

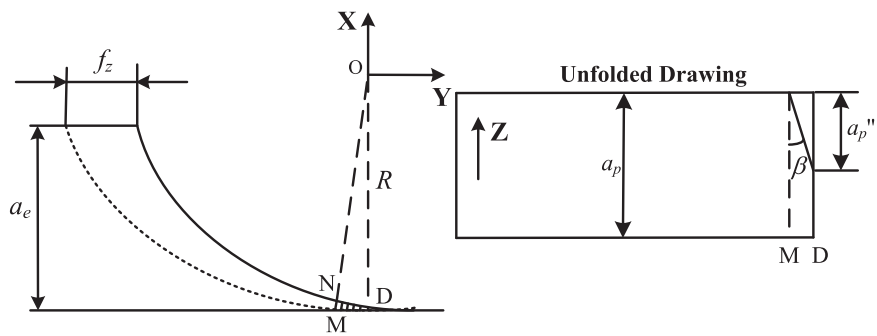

Fig. 7. 3rd cutting edge.

Table 1
Chemical composition of aluminum alloy Al7050-T7451.

Cr	Cu	Fe	Mg	Mn	Si	Ti	Zn	Zr	Al
≤ 0.04	2.0–2.6	≤ 0.15	1.9–2.6	≤ 0.1	≤ 0.12	≤ 0.06	5.7–6.7	0.08–0.15	balance

Table 2
Mechanical properties of aluminum alloy Al7050-T7451.

Density	2.83 g/mm^3	Poisson's ratio	0.330
Hardness, Vickers	162	Shear modulus	26.9 GPa
Ultimate tensile strength	524 MPa	Shear strength	303 MPa
Tensile yield strength	469 MPa	Specific heat capacity	0.86 J/(g °C)
Elongation at break	11.0%	Thermal conductivity	157 W/(g °C)
Elasticity modulus	71.7 GPa	Melting point	488-629.4 °C

$$F_s = R\cdot\tau_s\cdot f_z\cdot\left[\cos(\theta-\omega\cdot t)-\cos\theta\right]/(\sin\varphi\cdot\tan\beta) \tag{19}$$

2.4.3. Cutting forces model in 2nd stage

As shown in Fig. 6, the uncut chip thickness is expressed as:

$$f(z,t) = f_z\cdot\sin(\theta-\omega\cdot t+z\cdot\tan\beta/R),\ 0\le z\le a_p \tag{20}$$

The differential sliced layers are integral along the direction of cutting edge (Z direction) and the total shear force is expressed as:

$$F_s = R\cdot\tau_s\cdot f_z\cdot\left[\cos(\theta-\omega\cdot t)-\cos(\theta-\omega\cdot t+\gamma)\right]/(\sin\varphi\cdot\tan\beta) \tag{21}$$

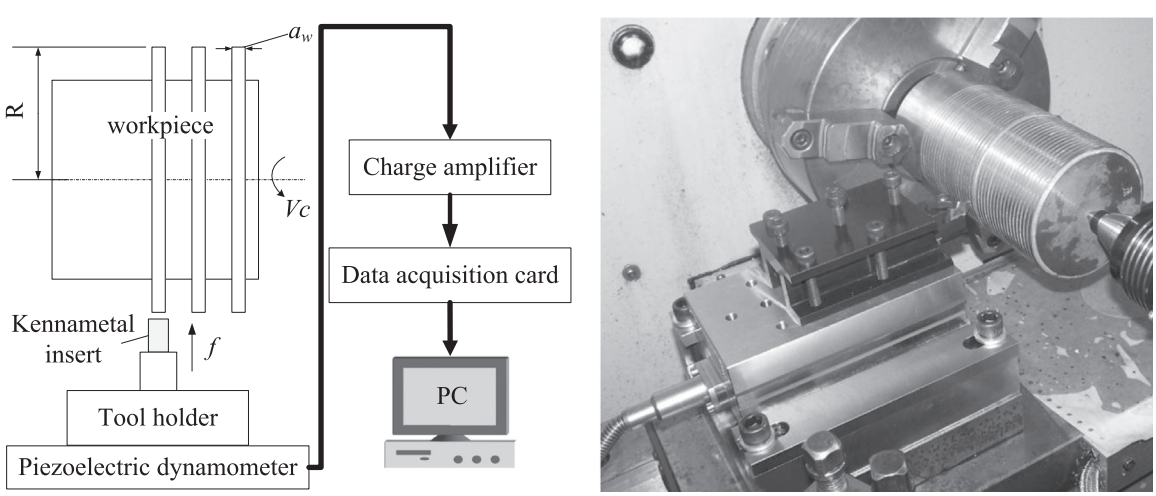

Fig. 8. Schematic of the experimental set-up.

Table 3
Cutting parameters of turning experiments.

Experiments No.	α (°)	v_c (m/min)	f (mm/rev)	a_w (mm)
1	0	170	0.08	3.02
2	0	170	0.09	3.22
3	0	170	0.1	3.10
4	0	170	0.11	3.14
5	0	170	0.12	3.12
6	0	85	0.1	3.00
7	0	134	0.1	2.58
8	0	170	0.1	2.28
9	0	211	0.1	2.26
10	0	264	0.1	2.34
11	5	85	0.1	2.80
12	5	134	0.1	2.02
13	5	170	0.1	2.42
14	5	211	0.1	2.22
15	5	264	0.1	2.16
16	10	85	0.1	2.42
17	10	134	0.1	2.12
18	10	170	0.1	2.42
19	10	211	0.1	2.52
20	10	264	0.1	2.18

Table 4
Turning forces and chip thickness.

Experiments no.	F_c (N)	F_t (N)	β_α (°)	t_c (mm)	ϕ (°)
1	79.6	49.3	31.77	0.141	29.57
2	83.7	50.0	30.85	0.152	30.63
3	99.8	58.7	30.46	0.162	31.69
4	114.9	63.5	28.93	0.179	31.57
5	118.7	66.9	29.41	0.196	31.48
6	124.1	69.9	29.39	0.199	26.68
7	113.6	66	32.50	0.188	28.01
8	99.8	58.7	30.46	0.162	31.69
9	90.6	53.3	30.47	0.159	32.17
10	92.7	55.0	30.68	0.151	33.51
11	117.1	69.3	35.62	0.196	28.01
12	109.7	65.2	35.73	0.180	30.18
13	103.5	58.3	34.39	0.168	32.02
14	97.6	52.7	33.37	0.152	34.81
15	95.8	50.8	32.94	0.149	35.38
16	111.3	56.7	37.00	0.181	31.04
17	104.1	51.3	36.23	0.168	33.18
18	96.6	45.5	35.22	0.154	35.78
19	90.1	43.2	35.62	0.141	38.54
20	85.8	38.9	34.39	0.130	41.16

2.4.4. Cutting forces model in 3rd stage

As shown in Fig. 7, the uncut chip thickness is expressed as:

$$f(z,t) = f_z \cdot sin(\theta - \omega \cdot t + z \cdot tan\beta / R),\ a_p - a_p'' \le z \le a_p \tag{22}$$

$$a_p'' = R \cdot (\theta - \omega \cdot t + \gamma) \cdot ctan\beta \tag{23}$$

The differential sliced layers are integral along the direction of cutting edge (Z direction) and the total shear force is expressed as:

$$F_s = R \cdot \tau_s \cdot f_z \cdot \left[1 - cos(\theta - \omega \cdot t + \gamma)\right] / (sin\varphi \cdot tan\beta) \tag{24}$$

3. Turning experiments and determination of material constant

3.1. The experimental set-up

The turning experiments were performed on the CAK6150 machine tool. Aerospace aluminum alloy Al7050-T7451 was selected as the workpiece material, which is subjected to heat

Table 5
Friction angle in the different cutting conditions.

Experiment no.	α (°)	v_f (m/min)	h (mm)	β_α (°)
1	0	96.45	0.08	31.77
2	0	100.66	0.09	30.85
3	0	104.94	0.1	30.46
4	0	104.47	0.11	28.93
5	0	104.08	0.12	29.41
6	0	42.71	0.1	29.39
7	0	71.28	0.1	32.50
8	0	104.94	0.1	30.46
9	0	132.70	0.1	30.47
10	0	174.83	0.1	30.68
11	5	43.37	0.1	35.62
12	5	74.44	0.1	35.73
13	5	101.19	0.1	34.39
14	5	138.82	0.1	33.37
15	5	177.18	0.1	32.94
16	10	46.96	0.1	37.00
17	10	79.76	0.1	36.23
18	10	110.39	0.1	35.22
19	10	149.65	0.1	35.62
20	10	203.08	0.1	34.39

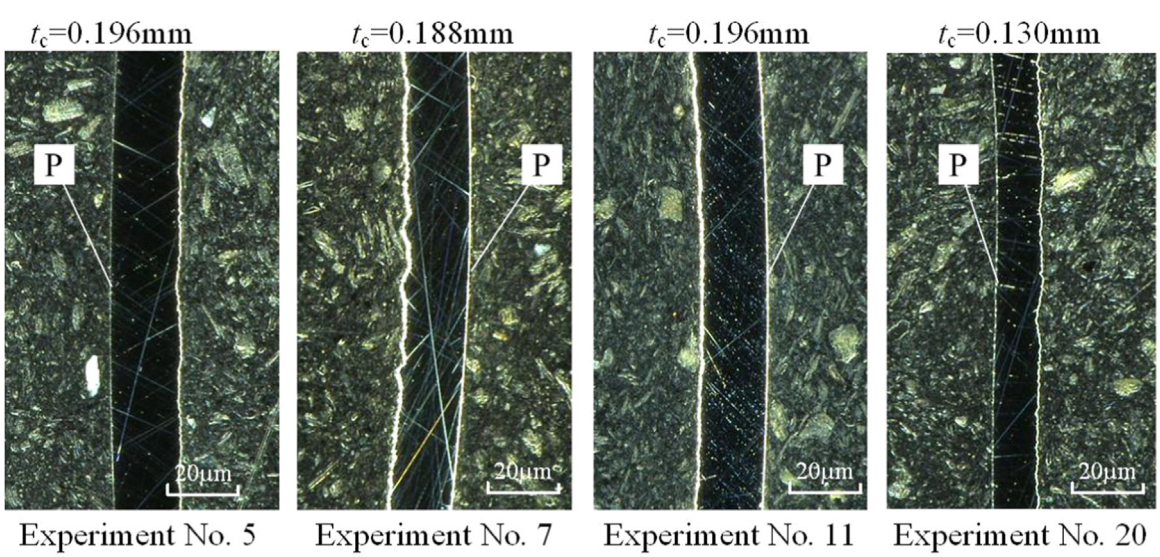

Fig. 9. Chip morphology.

Table 6
Shear angle models [29].

No.	Relationship models	Authors	Remarks
1	$\varphi=\pi/4+(\alpha-\beta_\alpha-C_1)/2$	Zvorikyn	C_1 is a constant, depending upon the shape of the outer boundary of the chip.
2	$\varphi=\pi/8+(\alpha-\beta_\alpha)/2$	Herman	
3	$\varphi=\pi/4+(\alpha-\beta_\alpha)$	Krystoff	
4	$\varphi=\pi/4+\alpha/2-\beta_\alpha$	Stabler	
5	$\varphi= C_0/2+(\alpha-\beta_\alpha)/2$	Merchant	C_0 is called as machinability constant, depending upon the material of workpiece.
6	$\varphi=\pi/4+(\alpha-\beta_\alpha)/2\text{-}\psi/2$	Zorev	ψ is the angle between the tangent to the upper boundary of the plastic zone at the point of its intersection with the specific shear plane and the cutting plane.
7	$\varphi=\pi/4+(\alpha-\beta_\alpha)+\eta'$	Shaw, Cook, Finnie	η' is called as the BUE angle, which varies with the cutting conditions.
8	$\varphi=\pi/4+\alpha-\tan^{-1}2\mu/2$	Hucks	
9	$\varphi=\alpha-\beta_\alpha+\tan^{-1}\{(1/2+\pi/4-\varphi)+[\cos(2\varphi-2\alpha)/\tan\beta_\alpha\text{-}\sin(2\varphi-2\alpha)]$	Oxley	
10	$\tan\varphi=\cos\alpha/[e^{\mu(\pi/2-\alpha)}\text{-}\sin\alpha]$	Kronenberg	
11	$\varphi=\{\sin^{-1}[\varepsilon\cdot\cos(\beta_\alpha\text{-}\alpha)+(1-\varepsilon)\cdot\sin(\beta_\alpha\text{-}\alpha)]\}/2+(\alpha-\beta_\alpha)/2$	Widal	ε is a workpiece material dependent constant.

Table 7
Turning forces and chip thickness.

Exp. no.	$2\varphi+2\beta_\alpha\text{-}\alpha$	$2\varphi+\beta_\alpha\text{-}\alpha$	$\varphi+\beta_\alpha\text{-}\alpha$	ε-Widal	Error- Hucks	Error- Kronenberg	Error- Oxley
1	122.68	90.91	61.34	1.463	10.11	8.86	24.87
2	122.97	92.11	61.48	1.407	10.67	9.26	27.31
3	124.30	93.84	62.15	1.383	11.50	10.03	31.17
4	121.00	92.07	60.50	1.317	10.50	8.80	27.09
5	121.77	92.36	60.88	1.337	10.69	9.06	27.77
6	112.14	82.75	56.07	1.317	5.88	4.25	8.95
7	116.33	86.17	58.17	1.367	7.65	6.13	15.26
8	124.30	93.84	62.15	1.383	11.50	10.03	31.17
9	125.27	94.80	62.64	1.379	11.99	10.52	33.44
10	128.39	97.71	64.20	1.374	13.45	12.02	40.57
11	122.25	86.64	58.63	1.392	5.55	8.47	12.33
12	126.81	91.09	60.91	1.402	7.78	10.72	19.71
13	127.83	93.44	61.41	1.334	8.95	11.59	23.65
14	131.35	97.99	63.18	1.273	11.21	13.62	32.93
15	131.63	98.69	63.32	1.253	11.55	13.87	34.53
16	126.07	89.08	58.04	1.249	4.26	10.93	11.41
17	128.82	92.58	59.41	1.224	6.02	12.49	16.65
18	132.01	96.79	61.00	1.185	8.13	14.33	23.84
19	138.31	102.69	64.16	1.157	11.08	17.39	36.14
20	141.11	106.72	65.55	1.094	13.09	19.08	45.76
SD	6.56	5.44	2.29	0.093	2.58	3.39	9.71
AV	126.27	93.61	61.26	1.314	9.58	11.07	26.23
ξ	0.052	0.058	**0.037**	0.071	0.269	0.306	0.370

Table 8
Shear stress in the different cutting conditions.

Experiment no.	v_s (m/min)	h (mm)	τ_s (MPa)
1	195.46	0.08	276.99
2	197.57	0.09	263.50
3	199.78	0.1	284.12
4	199.53	0.11	307.70
5	199.33	0.12	288.50
6	95.13	0.1	356.97
7	151.78	0.1	325.44
8	199.78	0.1	284.12
9	249.26	0.1	257.23
10	316.64	0.1	259.07
11	92.00	0.1	332.67
12	147.51	0.1	311.95
13	190.11	0.1	301.38
14	242.25	0.1	285.72
15	304.85	0.1	281.95
16	89.69	0.1	340.97
17	143.55	0.1	323.18
18	185.93	0.1	302.66
19	236.53	0.1	271.39
20	303.84	0.1	256.62

Table 9
Orthogonal array of cutting parameters.

Experiment no.	n (rev/min)	f_z (mm/rev)	a_e (mm)	a_p (mm)
1	3000	0.04	4	2
2	3000	0.07	6	4
3	3000	0.1	8	6
4	4000	0.04	6	6
5	4000	0.07	8	2
6	4000	0.1	4	4
7	5000	0.04	8	4
8	5000	0.07	4	6
9	5000	0.1	6	2

treatment: annealing at 413 °C; solution at 477 °C; aging at 121-177 °C. The chemical composition and mechanical properties are given by Tables 1 and 2 [28], respectively.

The workpiece was pre-cut for the orthogonal cutting, as shown in Fig. 8. The Kennametal top notch inserts were used in these experiments. The material of cutting tool is K313 without coating to provide a sharp cutting edge with cutting edge radius 5 μm. There were three types cutting tools with the different rake

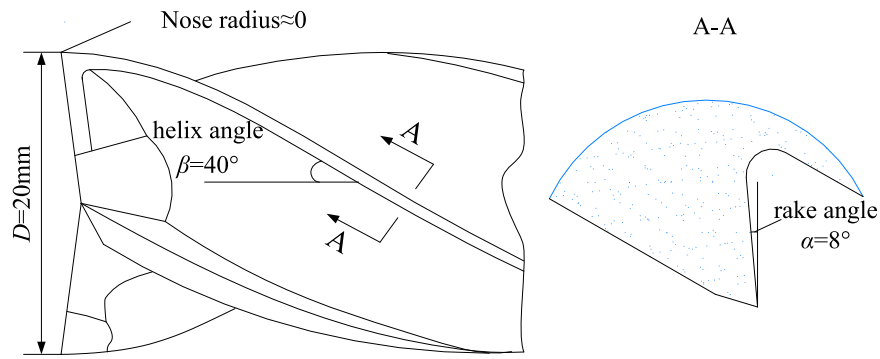

Fig. 10. Cutting tool geometry.

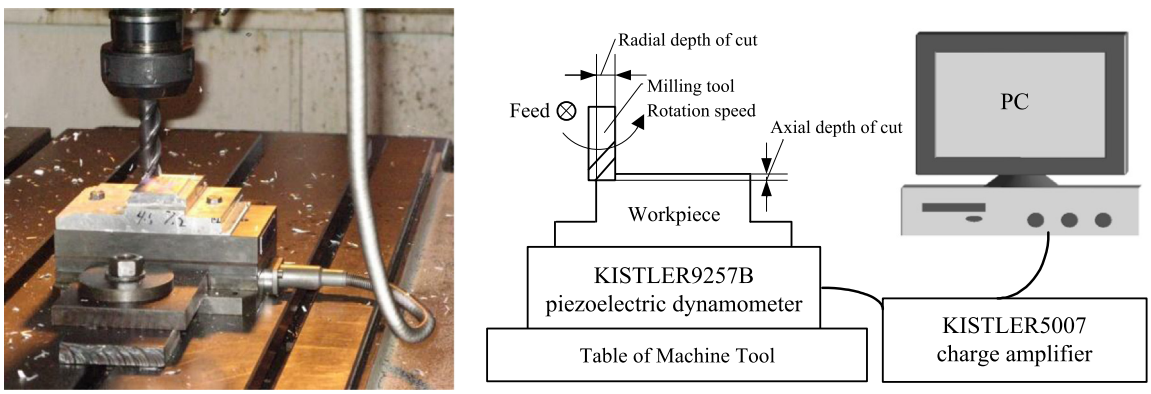

Fig. 11. Schematic of measurement and machining system. (a) Experimental result. (b) Calculated result.

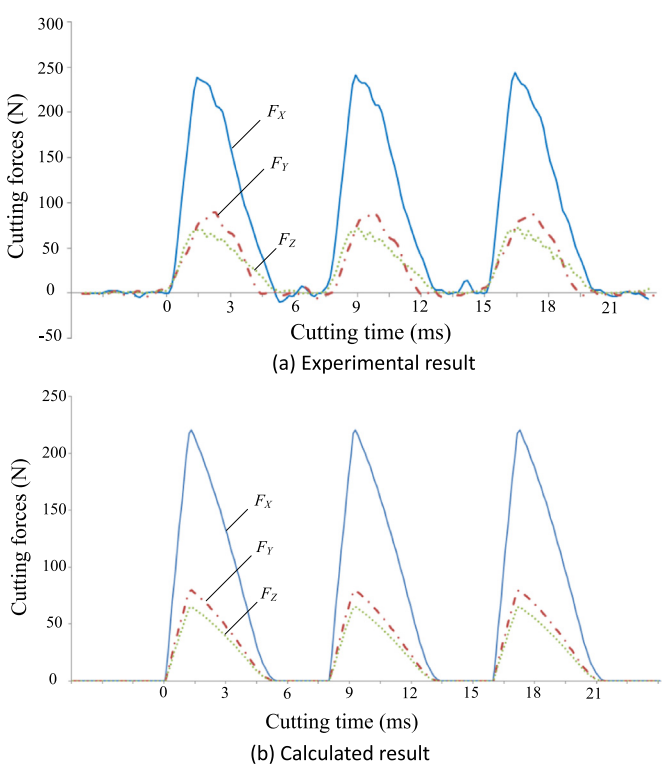

Fig. 12. The experimental result and calculated result (experiment No. 2).

angles of 0°, 5° and 10° respectively. The flank angle was 7°. The parameters design of experiments was shown in Table 3. New inserts were used in every cut to avoid the effect of tool wear.

The design of experiments considered the different rake angle, cutting speed and feed rate, the cutting parameters were listed in the Table 3. The width of cut in every cut is namely the width of the thin section of sample. They were pre-measured and listed in the Table 3, too.

3.2. Measurement of turning forces and chip thickness

The chips were selected and embedded for the investigation of the chip thickness t_c, as Fig. 9 shown. The side of chips which were marked with P contacts with cutting tools. The shear angle can be calculated according to the Eq. (8).

The cutting forces were measured by the piezoelectric dynamometer, five times in every cut. The average values of turning forces were calculated to decrease the experimental error. The unit cutting forces were calculated as the ratio of cutting forces and width of cut. The apparent friction angles were calculated according to the following equation:

$$\beta_\alpha = \alpha + arctan\left(F_t/F_n\right) \tag{25}$$

Where β_α is the apparent friction angles, F_t is the unit thrust forces and F_c is the unit cutting force.

F_t/F_n is associated with h and v_f, equation is also expressed as:

$$\beta_\alpha = \alpha + arctan\left(h^i \cdot v_f{}^j\right) \tag{26}$$

Where i and j are the exponent of h and v_f respectively. The measurement results were listed in Table 4.

3.3. Determination of friction angle

The data in Table 5 were employed to fit the Eq. (26). The fit results showed the sliding velocity and uncut chip thickness were significantly correlated and the fit precision is 98.5%. The relationship between friction angle and sliding velocity, uncut chip thickness was expressed as:

Table 10
Maximal cutting forces comparison of experimental result and calculated result.

No.	F_{Xmax}			F_{Ymax}			F_{Zmax}			Average error (%)
	E (N)	C (N)	Error (%)	E (N)	C (N)	Error (%)	E (N)	C (N)	Error (%)	
1	101	62	38.61	50	26	48.00	21	15	28.57	38.40
2	238	221	7.14	94	80	14.89	70	65	7.14	9.73
3	491	479	2.44	142	157	10.56	134	158	17.91	10.31
4	216	182	15.74	96	75	21.88	55	45	18.18	18.60
5	129	119	7.75	50	43	14.00	45	35	22.22	14.66
6	495	448	9.49	160	148	7.50	115	146	26.96	14.65
7	175	134	23.43	71	55	22.54	42	34	19.05	21.67
8	236	215	8.90	96	78	18.75	76	64	15.79	14.48
9	149	138	7.38	55	47	14.55	53	44	16.98	12.97
Average error (%)		13.43				19.18			19.20	17.27

Remark: E represents the experimental results, C represents the calculated results.

Table 11
Statistical analysis of calculated error.

Variance source	P-value			
	Error-F_{Xmax}	Error-F_{Ymax}	Error-F_{Zmax}	Error-Average
Rotation speed	0.253	0.726	0.760	0.931
Feed per tooth	**0.002**	**0.018**	0.782	**0.023**
Axial depth of cut	0.050	0.285	0.535	0.170
Radial depth of cut	**0.032**	0.421	0.640	0.178

$$\beta_\alpha = arctan\left(0.3125\cdot h - \ - 0.2307\cdot v_f^{0.02128}\right) + 0.543\cdot\alpha \tag{27}$$

3.4. Determination of shear angle

Many researchers proposed the relationship models among shear angle φ, friction angle β_α and rake angle α. There are some simply relationship model which can predict the shear angle from the cutting process parameters itself without extensive experiments [29], as listed in Table 6.

The model No. 1, 2, 5, 6 can be expressed as:

$$2\varphi + \beta_\alpha - \alpha = C \tag{28}$$

The model No. 3 can be expressed as:

$$\varphi + \beta_\alpha - \alpha = C \tag{29}$$

The model No. 4 can be expressed as:

$$2\varphi + 2\beta_\alpha - \alpha = C \tag{30}$$

where C is a material dependent constant.

According to the Eqs. (28)–(30) and model (11) in Table 6, the material dependent constant C and ε were calculated by the data in the different cutting condition. According to the model (8)–(10) in Table 6, the errors between calculated results and experiment results were calculated. The average value (AV) and standard deviation (SD) of constants and errors in the different relationship models were calculated. The ratios ξ of standard deviation to average value were employed to select the most reasonable relationship model. The calculated results were shown in Table 7.

It found Eq. (29) and the experimental results is the best consistent. Introducing the Eq. (29) into Eq. (3),

$$\tau_s = F_c\cdot sin\left(C - \beta_\alpha + \alpha\right)\cdot cosC/h/a_w/cos\left(\beta_\alpha - \alpha\right) \tag{31}$$

τ_s is the function of v_s, Eq. (31) is also expressed as:

$$\tau_s = m\cdot v_s^{\,n}, \tag{32}$$

where m and n are the coefficient and exponent of v_s respectively.

The calculated results of shear stress τ_s were listed in Table 8.

The data in Table 8 were employed to fit the Eq. (32). After the first fit process, it found that the uncut chip thickness was not significantly correlated. So the item uncut chip thickness h was removed and the fit process was performed again. The second fit showed the shear velocity was significantly correlated and the fit precision is 83.7%. The relationship between shear stress and shear velocity was expressed as:

$$\tau_s = 985.85\cdot v_s^{-0.23055} \tag{33}$$

4. Milling experiments and error analysis of milling force model

4.1. Milling experiments

The single factor experiments are performed in order to validate the theoretical model. The orthogonal array was employed in the design of experiments, as Table 9 shown.

The machine tool is DAEWOO V500 machining center. The cutting tool is Seco 35XL200 milling tool, as shown in Fig.10. The workpiece material is Aerospace aluminum alloy Al7050-T7451. The cutting forces are measured using a three-component piezoelectric dynamometer (Kistler 9257 B). A charge amplifier (Kistler 5007) converts the electrical charge into a proportional voltage, as Fig. 11 shows. The comparison of experimental result and theoretically calculated result (Experiment no. 2) was shown in Fig. 12.

Actually,. The maximal cutting forces and when they occur are worthy of attention. The maximal cutting forces F_{Xmax}, F_{Ymax}, F_{Zmax} were listed in Table 10. Most experimental results show good agreement with the theoretically calculated results.

4.2. Error analysis

Most theoretically calculated results were in good agreement with the experimental results, but some showed bad agreement. The statistical analysis of variance (ANOVA) was performed to see which cutting parameters were statistically significant to the calculated error. The analysis results were listed in the Table 11.

The P-value is the probability of obtaining a test statistic that is at least as extreme as the actual calculated value. The more small P-value the more better correlation. Generally the item with P-value lower than 0.05 is considered to be significantly correlated. For the error of F_{Xmax}, the feed per tooth and radial depth of cut are significantly correlated, namely the feed per tooth and radial depth of cut effect the precision of F_X theoretical cutting forces model greatly. For the error of F_{Ymax}, only the feed per tooth is significantly correlated, namely the feed per tooth effects the

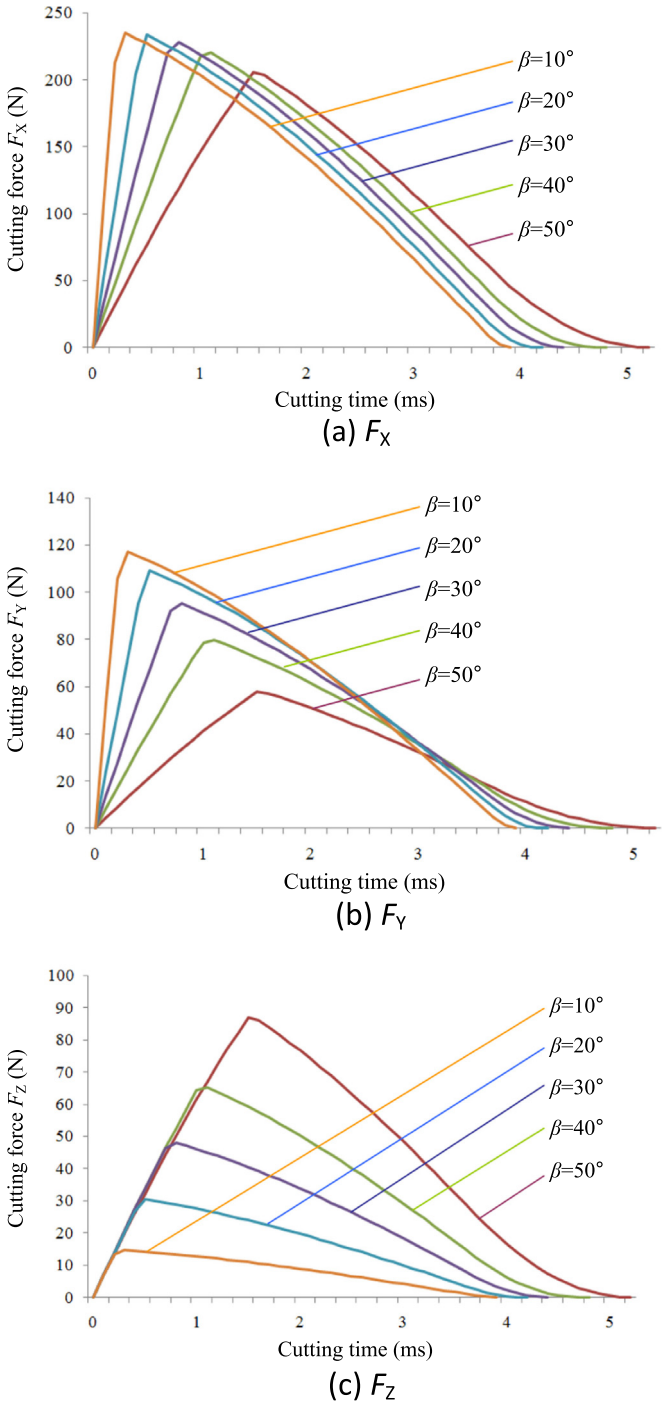

Fig. 13. Effect of helix angle on the cutting forces. (N=3000 rev/min, f_z=0.07 mm/rev, a_e=6 mm, a_p=4 mm, α=8°).

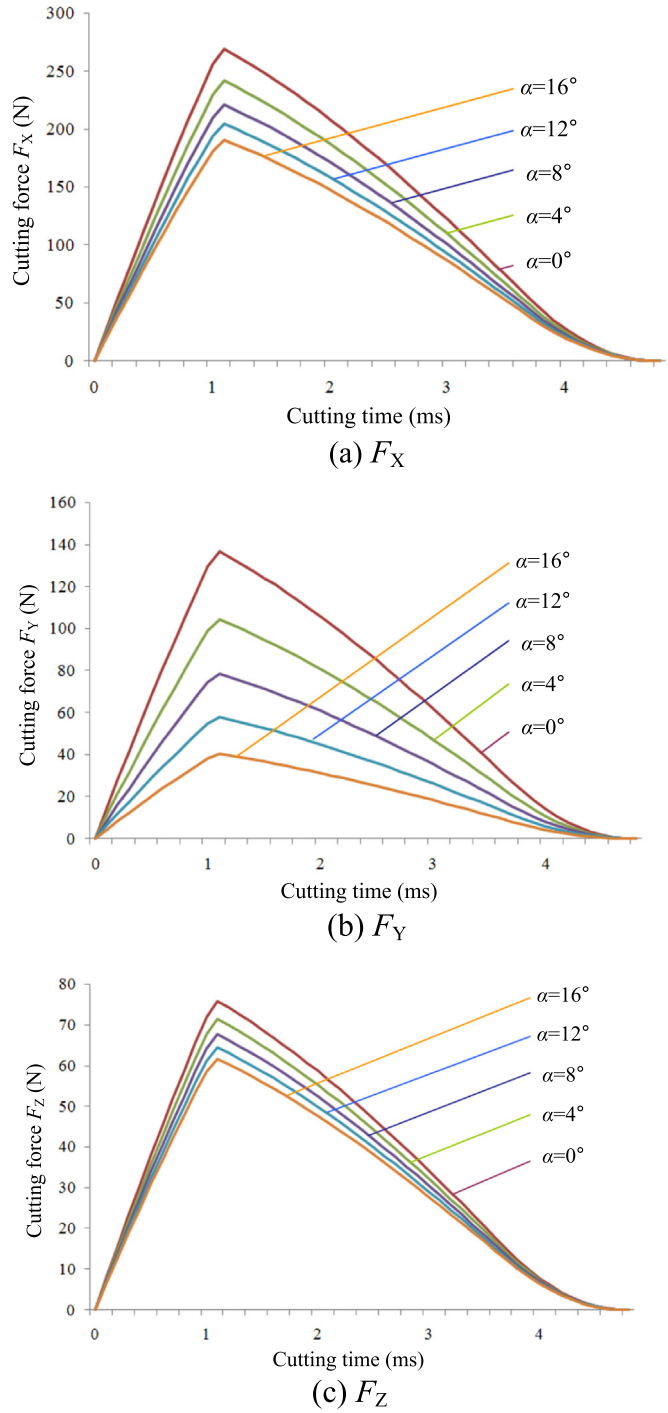

Fig. 14. Effect of rake angle on the cutting forces. (N=3000 m/min, f_z=0.07 mm/rev, a_e=6 mm, a_p=4 mm, β=40°).

precision of F_Y theoretical cutting forces model greatly. For the error of F_{Zmax}, no cutting parameter is significantly correlated. For the error of average error, only the feed per tooth is significantly correlated, namely the feed per tooth effects the precision of theoretical cutting forces model greatly.

As reported above, the feed per tooth is the first factor to influece the precision of cutting forces calculation. And the error increase with the decrease of the feed per tooth. The cutting tool is considered as absolutly sharp but actually the edge radius exists. When the feed per tooth or uncut chip thickness is small, the influence of edge radis can not be neglected. The error of theoretically calculated results increases. So this theoretical model cannot work well when the uncut chip thickness is small. However, the prediction precision of proposed theoretical model of cutting forces is acceptable (average error 17.27%).

5. Effect of milling tool geometries and milling parameters on milling forces

5.1. Effect of helix angle β

As shown in Fig. 13, F_X decreases with the increase of helix angle. F_Y decreases obviously with the increase of helix angle in

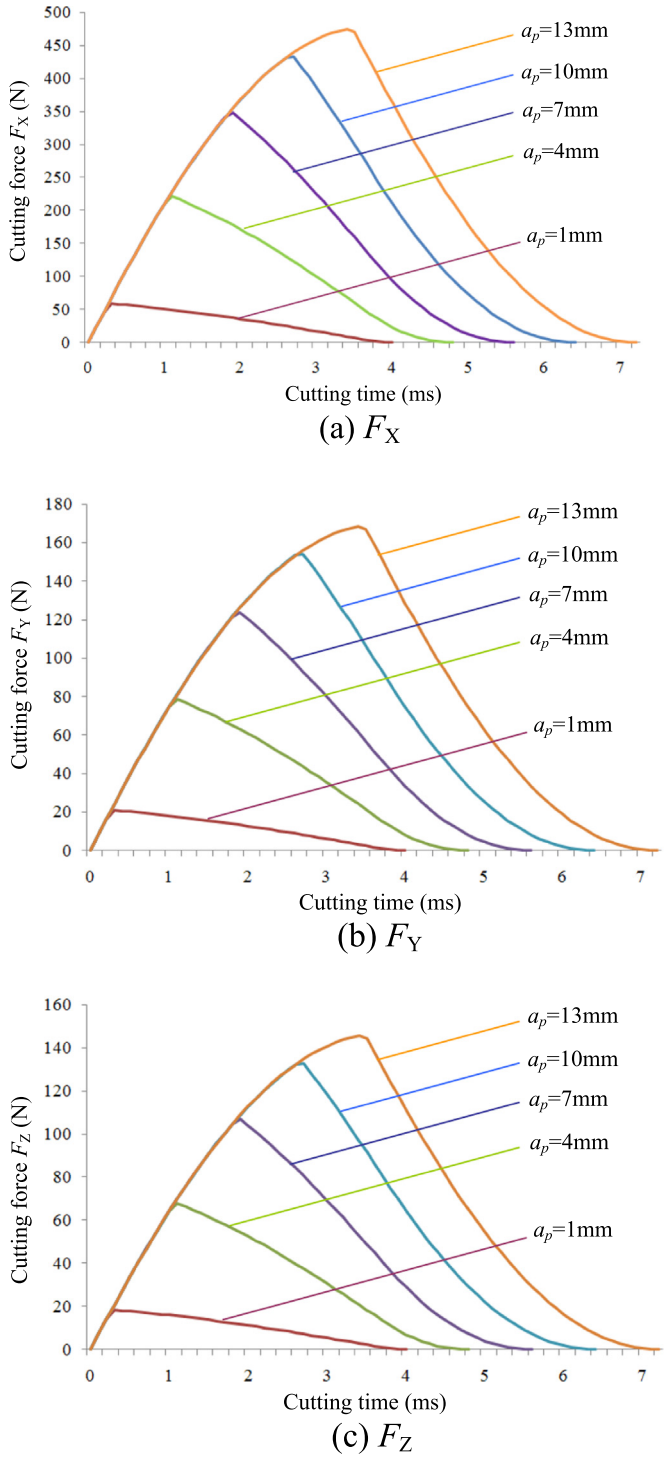

Fig. 15. Effect of axial depth of cut on the cutting forces. (N=3000 m/min, f_z =0.07 mm/rev, a_e=6 mm, β=40°, α=8°).

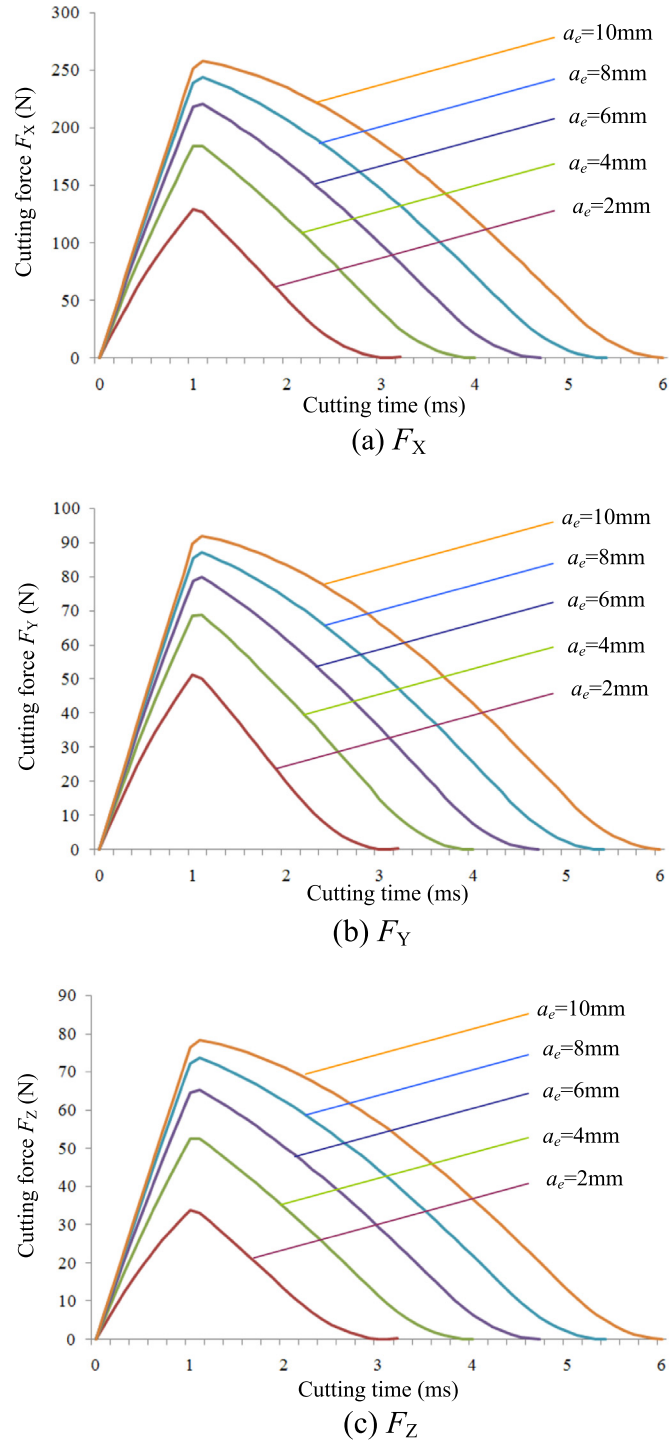

Fig. 16. Effect of radial depth of cut on the cutting forces. (N=3000 rev/min, f_z =0.07 mm/rev, a_p=4 mm, β=40°, α=8°).

the beginning of milling process, which benefits the dimension error control in the machining of parts with low rigid structure in the Y direction. But the falling extend of milling force F_Y after force peak decreases with the increase of helix angle, even the milling force F_Y of helix angle 50° becomes the biggest one after cutting time 3 ms, as shown in Fig. 13 (b). The axial forces F_Z increases greatly with the increase of helix angle. But the duration time from cut-in to maximal cutting forces increases with the increase of helix angle, which benefits the cutting stability. The effect of helix angle on milling forces F_Y and F_Z is more obvious than that on milling force F_X.

5.2. Effect of rake angle α

As shown in Fig. 14, both F_X and F_Y decrease with the increase of rake angle. F_Y decreases obviously, which benefits the dimension error control in the machining of parts with low rigid structure in the Y direction. The axial forces F_Z increases with the increase of rake angle. The duration time from cut-in to maximal cutting forces does not change. The effect of rake angle on milling forces F_Y is more obvious than that on milling force F_X and F_Z.

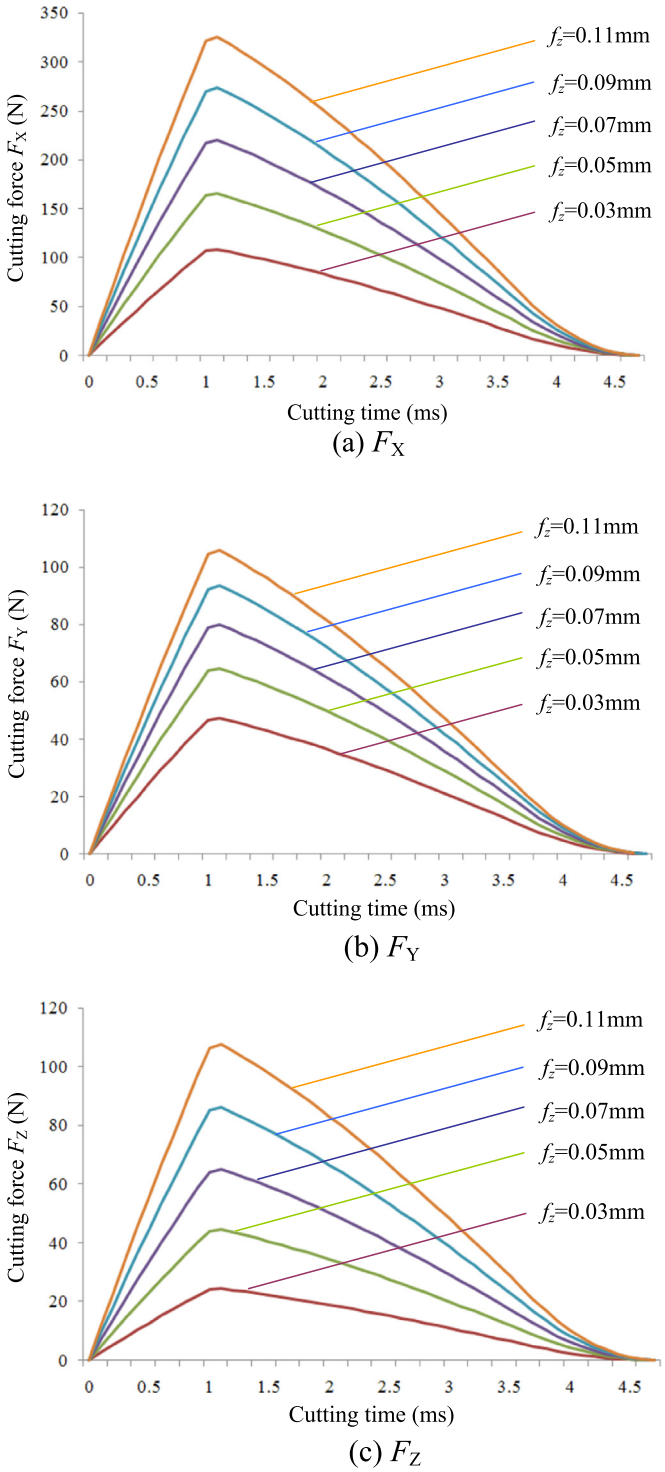

Fig. 17. Effect of feed rate on the cutting forces. (N=3000 rev/min, a_p=4 mm, a_e=6 mm, β=40°, α=8°).

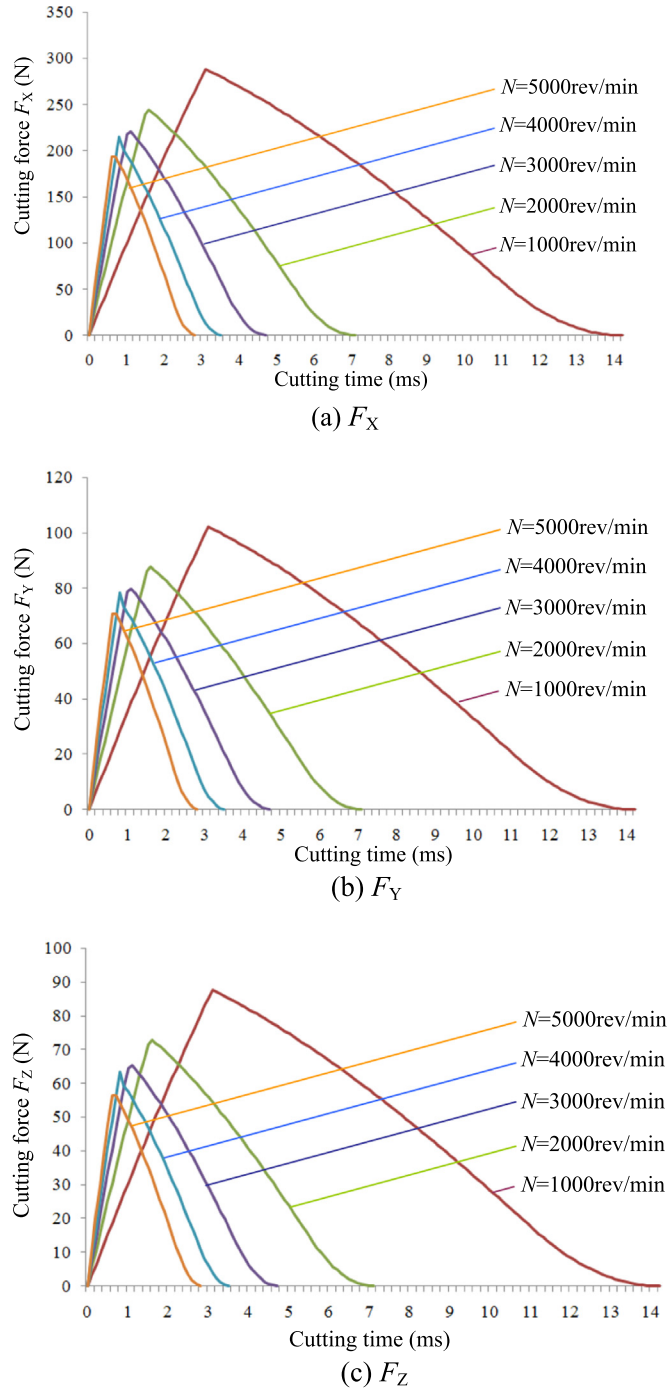

Fig. 18. Effect of rotation speed on the cutting forces. (f_z=0.07 mm/rev, a_p=4 mm, a_e=6 mm, β=40°, α=8°).

5.3. Effect of axial depth of cut a_p

As shown in Fig. 15, cutting forces F_X, F_Y and F_Z increase with the increase of axial depth of cut. But the ratios of cutting forces to axial depth of cut decrease with the increase of axial depth of cut. With the increase of axial depth of cut, the duration time from cut-in to maximal cutting forces increases, which benefits the cutting stability. The effect of axial depth of cut on milling forces F_X, F_Y and F_Z is same.

5.4. Effect of radial depth of cut a_e

As shown in Fig. 16, cutting forces F_X, F_Y and F_Z increase with the increase of radial depth of cut, because the maximal uncut chip thickness increases with the increase of radial depth of cut. The duration time from cut-in to maximal cutting forces does not change. The effect of radial depth of cut on milling forces F_X, F_Y and F_Z is same.

5.5. Effect of feed rate per tooth F_Z

As shown in Fig. 17, cutting forces F_X, F_Y and F_Z increase with the increase of feed rate. But the ratios of cutting forces F_X, F_Y to

feed rate decrease with the increase of feed rate. The ratio of cutting forces F_Z to feed rate increases with the increase of feed rate, because the friction angle decreases with the increase of feed rate, as Eq. (15) shown. The duration time from cut-in to maximal cutting forces does not change. The effect of feed rate per tooth on milling forces F_X, F_Y and F_Z is same.

5.6. Effect of rotation speed N

As shown in Fig. 18, cutting forces F_X, F_Y and F_Z decrease with the increase of rotation speed, because the shear stress and friction angle decrease with the increase of rotation speed, as Eqs. (15) and (17) shown. So the high speed cutting can decrease the cutting forces and benefit the cutting processes. The effect of rotation speed on milling forces F_X, F_Y and F_Z is same.

6. Conclusions

- The sculptured shear surface in the milling processes was proposed to analyze the engagement of milling tool and workpiece. And the analytical model of milling forces was built, considering the effect of friction and shear stress.
- The statistic models of shear angle, friction angle and shear stress were built based on the chip thickness and turning forces from turning experiments.
- The milling experiments validated the accuracy of proposed milling forces model.
- The effect of helix angle, rake angle, axial depth of cut, radial depth of cut, feed rate and rotation speed on milling forces were analyzed. The effect extent of cutting tool geometrical parameters on milling forces in the different direction is very different, while the effect extent of milling parameters on milling forces in the different direction is same.

Acknowledgments

This study is funded by National Natural Science Foundation (No. 51475173), the Major Project on the Integration of Industry and Research of Fujian Province (No. 2014H6018), Cultivation Project for Distinguished Young Talents in the Fujian Province (No. JA14013), Industry-University Cooperation Project of Xiamen City (No. 3502Z20163012).

References

[1] Yoon Hae-Sung, Lee Jang-Yeob, Kim Min-Soo, Ahn Sung-Hoon. Empirical power-consumption model for material removal in three-axis milling. J Clean Prod 2014;Volume 78:54–62 1 September.
[2] Budak E, Altintaş Y, Armarego EJA. Prediction of milling force coefficients from orthogonal cutting data. J Manuf Sci E-T ASME, 188; 1996. p. 216–24.
[3] Newby G, Venkatachalam S, Liang SY. Empirical analysis of cutting force constants in micro-end-milling operations. J Mater Process Technol 2007; Volumes 192–193:41–7 1 October.
[4] Li Ning Stephen C Veldhuis. Mechanistic modeling of ball end milling including tool wear. J Manuf Process 2006;Volume 8(Issue 1):21–8.
[5] Wang Shih-Ming, Chiou Chu-Hsiang, Cheng Yuan-Ming. An improved dynamic cutting force model for end-milling process. J Mater Process Technol 2004; Volume 148(Issue 3):317–27 30 May.
[6] Zhou L, Peng FY, Yan R, Yao PF, Yang CC, Li B. Analytical modeling and experimental validation of micro end-milling cutting forces considering edge radius and material strengthening effects. Int J Mach Tools Manuf 2015;97:29–41.
[7] Jiang F, Yan L, Rong Y. Orthogonal cutting of hardened AISI D2 steel with TiAlN-coated inserts—simulations and experiments. Int J Adv Manuf Technol 2013;64:1555–63.
[8] Chang CS. Prediction of the cutting temperatures of stainless steel with chamfered main cutting edge tools. J Mater Process Tech 2007;190:332–41.
[9] Malakizadi A, Cedergren S, Sadik I, Nyborg L. Inverse identification of flow stress in metal cutting process using Response Surface Methodology. Simul Model Pract Theory 2016;60:40–53.
[10] Cheng X, Zha X, Jiang F. Optimizing the geometric parameters of cutting edge for rough machining Fe-Cr-Ni stainless steel. Int J Adv Manuf Technol 2015.
[11] Xie LJ, Schmidt J, Schmidt C, Biesinger F. 2D FEM estimate of tool wear in turning operation. Wear 2005;258:1479–90.
[12] Outeiro JC, Umbrello DM, Saoubi R. Experimental and numerical modelling of the residual stresses induced in orthogonal cutting of AISI 316L steel. Int J Mach Tools Manuf 2006;46:1786–94.
[13] Soo SL, Aspinwall DK, Dewes RC. 3D FE modelling of the cutting of Inconel 718. J Mater Process Technol 2004;150:116–23.
[14] Zel TR, Altan T. Process simulation using finite element method — prediction of cutting forces, tool stresses and temperatures in high-speed flat end milling. Int J Mach Tools Manuf 2000;40:713–38.
[15] Jiang F, Li JF, Rong YM, Sun J, Zhang S. Study of Cutting Temperature in Cold-Air Milling of Ti6Al4V Alloy.
[16] Jiang F, Li J, Sun J, Zhang S, Wang Z, Yan L. Al7050-T7451 turning simulation based on the modified power-law material model. Int J Adv Manuf Technol 2010;48:871–80.
[17] Childs THC. Friction modelling in metal cutting. WEAR 2006;260:310–8.
[18] Jiang F, Zhang T, Yan L. Estimation of temperature dependent heat transfer coefficients in near-dry Cutting. Int J Adv Manuf Technol 2016.
[19] Buchkremer S, Wu B, Lung D, Münstermann S, Klocke F, Bleck W. FE-simulation of machining processes with a new material model. J Mater Process Technol 2014;214:599–611.
[20] Shaw MC. Metal cutting principles.NY, USA: Oxford University Press; 2005. p. 17–8.
[21] Shaw MC. Metal cutting principles.NY, USA: Oxford University Press; 2005. p. 127–44.
[22] Jin X, Altintas Y. Slip-line field model of micro-cutting process with round tool edge effect. J Mater Process Technol 2011;211:339–55.
[23] Moufki A, Dudzinski D. An analytical thermo-mechanical modelling of peripheral milling process using a predictive machining theory. Adv Mater Res 2011;223:93–100.
[24] Rodríguez P, Labarga JE. A new model for the prediction of cutting forces in micro-end-milling operations. J Mater Process Technol 2013;213:261–8.
[25] Shaw MC. Metal cutting principles.NY, USA: Oxford University Press; 2005. p. 18–20.
[26] Shaw MC. Metal cutting principles.NY, USA: Oxford University Press; 2005. p. 28–31.
[27] Shaw MC. Metal cutting principles.NY, USA: Oxford University Press; 2005. p. 392–4.
[28] Matweb. Material property data.; 2015. 〈http://www.matweb.com/search/DataSheet.aspx?MatGUID=142262cf7fbc4c83917ca5c3d17df1ed&ckck=1〉.
[29] Rao PN. Manufacturing technology-metal cutting & machine tools.OH, USA: McGraw-Hill Companies; 2000. p. 35–41.